Draft version June 21, 2013
Preprint typeset using LaTeX style emulateapj v. 5/2/11

COSMOLOGY FROM GRAVITATIONAL LENS TIME DELAYS AND PLANCK DATA

S. H. Suyu[1], T. Treu[2,*], S. Hilbert[3], A. Sonnenfeld[2], M. W. Auger[4], R. D. Blandford[5], T. Collett[4], F. Courbin[6], C. D. Fassnacht[7], L. V. E. Koopmans[8], P. J. Marshall[9,5], G. Meylan[6], C. Spiniello[8], M. Tewes[6]

Draft version June 21, 2013

ABSTRACT

Under the assumption of a flat ΛCDM cosmology, recent data from the Planck satellite point toward a Hubble constant that is in tension with that measured by gravitational lens time delays and by the local distance ladder. Prosaically, this difference could arise from unknown systematic uncertainties in some of the measurements. More interestingly – if systematics were ruled out – resolving the tension would require a departure from the flat ΛCDM cosmology, introducing for example a modest amount of spatial curvature, or a non-trivial dark energy equation of state. To begin to address these issues, we present here an analysis of the gravitational lens RXJ1131−1231 that is improved in one particular regard: we examine the issue of systematic error introduced by an assumed lens model density profile. We use more flexible gravitational lens models with baryonic and dark matter components, and find that the exquisite *Hubble Space Telescope* image with thousands of intensity pixels in the Einstein ring contains sufficient information to constrain these more flexible models. The total uncertainty on the time-delay distance is 6.5% for a single system, including the uncertainty over the two lens models considered. We thus proceed to combine our improved time-delay distance measurements with the WMAP9 and Planck posteriors. In an open ΛCDM model, the data for RXJ1131−1231 in combination with Planck favor a flat universe with $\Omega_k = -0.01 \pm 0.02$ (68% CI). In a flat wCDM model, the combination of RXJ1131−1231 and Planck yields $w = -1.55^{+0.19}_{-0.21}$ (68% CI).

Subject headings: galaxies: individual (RXJ1131−1231) — gravitational lensing: strong — methods: data analysis — distance scale

1. INTRODUCTION

The last few years have been hailed as the era of precision cosmology. Many different methods now point to the so-called concordance cosmology, characterized by a virtually flat geometry in a universe dominated by dark matter and dark energy (e.g., Hinshaw et al. 2012; Planck Collaboration et al. 2013). With precision on many parameters now reaching the few percent level, it is extremely valuable to compare and contrast different probes. A comparison between independent probes of similar precision is the cleanest way to test the accuracy of the measurements, and reveal unknown systematic uncertainties. Furthermore, certified tension between independent probes' measurements would require the falsification of the simplest models and potentially the discovery of new physics (Suyu et al. 2012).

A classic example is the interpretation of the cosmic microwave background (CMB) data. The power spectrum of the CMB anisotropies delivers an enormous amount of information about the high-redshift universe, but it is not directly sensitive to lower-redshift phenomena such as the rise of dark energy. Thus, inferring w or the Hubble constant (H_0) from CMB data typically requires strong assumptions about the cosmological model (e.g. flatness) or the combination with lower redshift probes. This is well exemplified by the Planck analysis (Paper XVI; Planck Collaboration et al. 2013). Assuming $\Omega_k = 0$ and $w = -1$, $H_0 = 67.3 \pm 1.2\,\mathrm{km\,s^{-1}\,Mpc^{-1}}$, in tension with that measured by various lower-redshift methods including the local distance ladder (Riess et al. 2011; Freedman et al. 2012), gravitational time delays (Suyu et al. 2013, hereafter SU13), and giant extragalactic H II regions (Chávez et al. 2012)[11]. In contrast, H_0 and w are virtually unconstrained by Planck data alone in a generic cosmology, thus erasing the tension. If confirmed, this tension would imply that the simplest flat ΛCDM is falsified. Given the high stakes, it is crucial to re-examine the uncertainties of each method, eliminating unaccounted for systematics.

The aim of this paper is two-fold. Firstly, we present a re-analysis of the gravitational lens system RXJ1131−1231 (Figure 1) discovered by Sluse et al. (2003). Following the work of Schneider & Sluse (2013, hereafter SS13) we consider composite mass models for the main deflector galaxy (Section 2). The composite models describe the stellar and dark matter components

suyu@asiaa.sinica.edu.tw
[1] Institute of Astronomy and Astrophysics, Academia Sinica, P.O. Box 23-141, Taipei 10617, Taiwan
[2] Department of Physics, University of California, Santa Barbara, CA 93106, USA
[3] Max-Planck-Institut für Astrophysik, Karl-Schwarzschild-Str. 1, 85748 Garching, Germany
[4] Institute of Astronomy, University of Cambridge, Madingley Rd, Cambridge, CB3 0HA, UK
[5] Kavli Institute for Particle Astrophysics and Cosmology, Stanford University, 452 Lomita Mall, Stanford, CA 94035, USA
[6] Laboratoire d'Astrophysique, Ecole Polytechnique Fédérale de Lausanne (EPFL), Observatoire de Sauverny, CH-1290 Versoix, Switzerland
[7] Department of Physics, University of California, Davis, CA 95616, USA
[8] Kapteyn Astronomical Institute, University of Groningen, P.O.Box 800, 9700 AV Groningen, The Netherlands
[9] Department of Physics, University of Oxford, Keble Road, Oxford, OX1 3RH, UK
[*] Packard Research Fellow

[11] except, e.g., the water masers (Reid et al. 2013)

separately, and are thus more realistic as well as more flexible than the single power-law models considered in our original analysis (SU13). We show that even with this broader class of lens models, the difference in the gravitational potential at locations of the multiple images of the quasars is extremely well constrained by the deep *Hubble Space Telescope* (*HST*) images of the Einstein ring and by the availability of multiple time delays. Section 3 discusses the impact of these flexible lens models on the measurement of the time-delay distance ($D_{\Delta t} \propto H_0^{-1}$), the combination of angular diameter distances constrained by time delays.

Secondly, having shown that uncertainties in the mass model are not significantly larger than our previous estimate, we proceed in Section 4 to combine our $D_{\Delta t}$ measurement with the recent CMB results from the Wilkinson Microwave Anisotropy Probe 9-year data (WMAP9; Hinshaw et al. 2012) and from Planck (Planck Collaboration et al. 2013). We find that RXJ1131−1231 is effective at breaking the CMB parameter degeneracies in constraining flatness and w. We conclude in Section 5.

Throughout this paper, each quoted parameter estimate is the median of the one-dimensional marginalized posterior probability density function (PDF), with the uncertainties showing, unless otherwise stated, the $16^{\rm th}$ and $84^{\rm th}$ percentiles (i.e., the 68% credible interval (CI)).

2. LENS MASS MODELS: POWER OF SPATIALLY EXTENDED EINSTEIN RINGS

SU13 modeled the lens galaxy in RXJ1131−1231 with a power-law mass distribution that was motivated by several studies, including the X-ray observations of galaxies (Humphrey & Buote 2010) and the lensing and kinematics analyses of galaxies in the Sloan Lens ACS survey (e.g., Koopmans et al. 2006; Gavazzi et al. 2007; Koopmans et al. 2009; Auger et al. 2010; Barnabè et al. 2011), which found that galaxies are well described by power-law mass distributions in regions covered by the data. Furthermore, the pixelated lens potential corrections applied by Suyu et al. (2009) to the gravitational lens B1608+656 was within ∼2% from a power law, validating the use of a simple power-law model. Here, we assess further the dependence of $D_{\Delta t}$ on the form of the mass model. In particular, we employ two other forms of the lens mass distribution that were considered by SS13: a cored power-law mass distribution, and a composite model of dark matter and baryons. In each case, we use the time delays from Tewes et al. (2012)[12] and the *HST* image showing the spatially extended images of the source galaxy (Figure 1; SU13) to constrain the lens model. The expressions for the likelihoods of the data are given in Section 6.2 of SU13.

2.1. *Cored power-law model*

The dimensionless surface mass density (convergence) of a cored power-law profile is given by

$$\kappa_{\rm cpl}(\theta_1,\theta_2) = \frac{3-\gamma'}{2}\left(\frac{\theta_{\rm E}}{\sqrt{q\theta_1^2+\theta_2^2/q+\theta_{\rm c}^2}}\right)^{\gamma'-1}, \quad (1)$$

[12] based on monitorings of COSMOGRAIL (COSmological MOnitoring of GRAvItational Lenses; e.g., Courbin et al. 2011; Tewes et al. 2013) and Kochanek et al. (2006) teams.

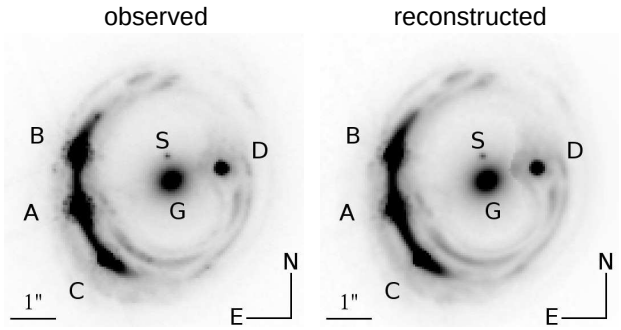

FIG. 1.— *HST* ACS image of RXJ1131−1231 in F814W filter. The background AGN is lensed into four images (A, B, C and D) by the primary lens galaxy G and its satellite S. Left: observed image. Right: reconstructed image based on the most probable composite model in Section 2.2.

where (θ_1,θ_2) are coordinates on the lens/image plane, γ' is the radial power-law slope (with $\gamma'=2$ corresponding to isothermal), $\theta_{\rm E}$ is the Einstein radius, q is the axis ratio of the elliptical isodensity contours, and $\theta_{\rm c}$ is the core radius. This is identical to the lens mass distribution used by SU13 except that now $\theta_{\rm c}$ is no longer set to zero.

Figure 1 shows a primary lens galaxy G and a satellite lens galaxy S that are surrounded by the Einstein ring of the lensed source. Following SU13 in the modeling procedure, we remodel the Advanced Camera for Surveys (ACS) image using the cored power-law profile for G. For simplicity, we fix the mass distribution of S to that of the most probable model in SU13 since the satellite impacts the $D_{\Delta t}^{\rm model}$ measurement at the <1% level. We also include an external shear contribution with strength $\gamma_{\rm ext}$ and position angle $\phi_{\rm ext}$. We use a grid of 50×50 source intensity pixels to model the spatially extended quasar host galaxy.

We sample the lens parameters and $D_{\Delta t}^{\rm model}$ using the same Markov chain Monte Carlo (MCMC) methods as were used in SU13. The lensing data constrain the maximum $\theta_{\rm c}$ to be $0.005''$ (95% CI), and $\theta_{\rm c}=0$ is compatible with the data. With such a small core radius allowed by the data, the marginalized values of the remaining lens parameters, $D_{\Delta t}^{\rm model}$ and the cosmological results are the same as those presented in SU13 within two significant digits.

2.2. *Composite mass model*

In the composite model, we treat baryons and dark matter individually. We model the baryonic mass distribution of the lens galaxy G as its observed light profile normalized by a constant M/L. The difference of two isothermal profiles mimics a Sersic profile (Dutton et al. 2011) and provides efficient computation of lensing quantities:

$$L(\theta_1,\theta_2) = \frac{L_0}{(1+q_{\rm L})}\Big[\frac{1}{\sqrt{\theta_1^2+\theta_2^2/{q_{\rm L}}^2+w_{\rm c}^2}} - \frac{1}{\sqrt{\theta_1^2+\theta_2^2/{q_{\rm L}}^2+w_{\rm t}^2}}\Big], \quad (2)$$

where $q_{\rm L}$ is the axis ratio, $w_{\rm c}$ and $w_{\rm t}$ are profile parameters with $w_{\rm t}>w_{\rm c}$. We use two sets of the above profile to fit the light distribution of G in the ACS image since a single one is inadequate (Claeskens et al. 2006; SU13). We impose common centroid and position angle for the

two sets of profiles. The light profile parameters for lens galaxy G are fixed to the optimized values. The light and mass profile of the satellite S are fixed to the most probable model in SU13 given its negligible impact. For the dark matter halo, we adopt the standard NFW profile (Navarro et al. 1996) whose three-dimensional density is

$$\rho(r) = \frac{\rho_0}{(r/r_{\rm s})(1+r/r_{\rm s})^2}, \quad (3)$$

where ρ_0 is a normalization and $r_{\rm s}$ is the scale radius. We follow Golse & Kneib (2002) for obtaining the deflection angles and lens potential of an elliptical NFW profile in projection.[13] As in the previous cases, we allow for an external shear contribution.

We have the following 10 parameters in modeling the ACS image and time delays: a global M/L of the baryons, the NFW parameters (centroid $(\theta_{1\rm h}, \theta_{2\rm h})$, axis ratio $q_{\rm h}$, position angle $\phi_{\rm h}$, normalization $\kappa_{0,\rm h}$, scale radius $r_{\rm s}$), external shear $\gamma_{\rm ext}$ and $\phi_{\rm ext}$, and the modeled time-delay distance $D_{\Delta t}^{\rm model}$.

Since $r_{\rm s}$ is in the 3-dimensional density in Equation (3), the projected surface mass density and thus $D_{\Delta t}$ are sensitive to $r_{\rm s}$. Unfortunately, $r_{\rm s}$ is poorly constrained by theory including baryonic physics. Thus we consider a broad range of plausible values: $r_{\rm s} = 4\farcs5$, $5\farcs6$, $6\farcs1$, $6\farcs6$, $7\farcs0$, $7\farcs5$, $8\farcs0$, $8\farcs4$, $8\farcs9$, $9\farcs4$, and $10\farcs5$. For each value, we sample using MCMC the remaining 9 parameters with a grid of 50×50 source intensity pixels.[14] We find that chains of different $r_{\rm s}$ values reproduce the ACS image comparably well given the pixel uncertainties in SU13. However, the time delays are not all well fitted. To be conservative, we combine the PDFs of the various $r_{\rm s}$ chains by weighting each with the likelihood of the time delays, as an approximate marginalization over $r_{\rm s}$.

The unmarginalized likelihood of the time delays peaks for $r_{\rm s} \sim 7\farcs5$. In the right-hand panel of Figure 1, we show the reconstructed *HST* image based on our most probable composite model with $r_{\rm s} = 7\farcs5$, which reproduces the global features of the observed image. In Figure 2, we show the circularly averaged convergence of the most probable model with $r_{\rm s} = 7\farcs5$. The shaded area is roughly the region spanned by the spatially extended arcs. Within this region, the combination of the baryons (dashed) and the dark matter (dotted) in the composite model yields a nearly perfect power-law profile. For comparison, the power-law model from SU13 is also plotted in solid. Therefore, the spatially extended arcs and the time delays provide strong constraints on the local profile of the lens mass distribution.

The composite model requires an external shear strength of $\gamma_{\rm ext} = 0.070 \pm 0.004$, which is lower than the 0.089 ± 0.006 for the power-law model, whereas the shear angles of the two models agree within 6°.

3. IMPACT ON TIME-DELAY DISTANCE

In Figure 3, we display $D_{\Delta t}^{\rm model}$ distributions for the two models: power law (dashed) and composite (dot dashed).

[13] Golse & Kneib (2002) introduced the ellipticity into the lens potential, and Sand et al. (2008) showed that this yields valid elliptical surface mass density when $q_{\rm h} \gtrsim 0.8$.

[14] For the case of $r_{\rm s} = 7\farcs0$, we tried a range of source resolutions (from 50×50 to 60×60) and find negligibly small shifts in $D_{\Delta t}^{\rm model}$ of $\lesssim 10\,{\rm Mpc}$.

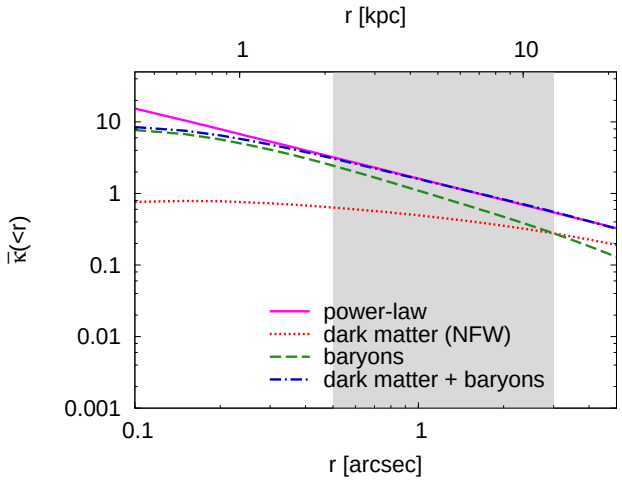

FIG. 2.— The circularly averaged convergence as a function of radius for the most probable models. The power-law model (solid) is from SU13. The composite model (dot-dashed) consists of a baryonic mass distribution based on the light profile (dotted), and a dark matter distribution based on an NFW profile (dashed). In the region covered by the Einstein ring, between $\sim 0.5''$ and $\sim 3''$, the slope of the composite model is nearly identical to that of the single power law. The spatially extended Einstein ring covering thousands of intensity pixels provide strong constraints on the local lens mass profile.

The dotted distributions correspond to the chains of various $r_{\rm s}$ values that are weighted by the time-delay likelihood; the higher the $r_{\rm s}$, the higher the $D_{\Delta t}^{\rm model}$. We conservatively assign equal priors to the two models (power-law and composite), on the grounds that we have no reason to believe one parametrization over another *a priori*. We show the combined $D_{\Delta t}^{\rm model}$ distribution in solid lines. The differences in the medians of the $D_{\Delta t}^{\rm model}$ distributions from this conservative model-averaging analysis are $< 3\%$.

The cosmological $D_{\Delta t}$ to the lens is affected by the external mass distributions along the line of sight and is related to the $D_{\Delta t}^{\rm model}$ from the lens modeling by

$$D_{\Delta t} = \frac{D_{\Delta t}^{\rm model}}{1-\kappa_{\rm ext}}, \quad (4)$$

where $\kappa_{\rm ext}$ characterizes the external convergence associated with these structures. Following SU13, we construct the PDF of $\kappa_{\rm ext}$ by ray tracing through the Millennium Simulation (Springel et al. 2005; Hilbert et al. 2009), selecting lines of sights in the simulations with a galaxy count around the lens system that is 1.4 times the average (measured by Fassnacht et al. 2011), and weighting by the external shear value. In Figure 4, we show the PDF of $\kappa_{\rm ext}$ for the two models, which differ by $\sim$0.02 due to the shear strengths.

Combining the $D_{\Delta t}^{\rm model}$ with the $\kappa_{\rm ext}$ PDF for each of the two lens models, we obtain via Equation (4) the PDF for $D_{\Delta t}$. The measured lens velocity dispersion of $323 \pm 20\,{\rm km\,s^{-1}}$ is used to further constrain the power-law model (SU13) and help break the mass-sheet degeneracy (e.g., Koopmans 2004). The full kinematics analysis of the composite model is beyond the current scope and deferred to future work.

A fitting formula for the PDF of $D_{\Delta t}$, which can be used to combine with any other independent data set, is

$$P(D_{\Delta t}|H_0, \Omega_{\rm de}, w, \Omega_{\rm m}) \simeq$$

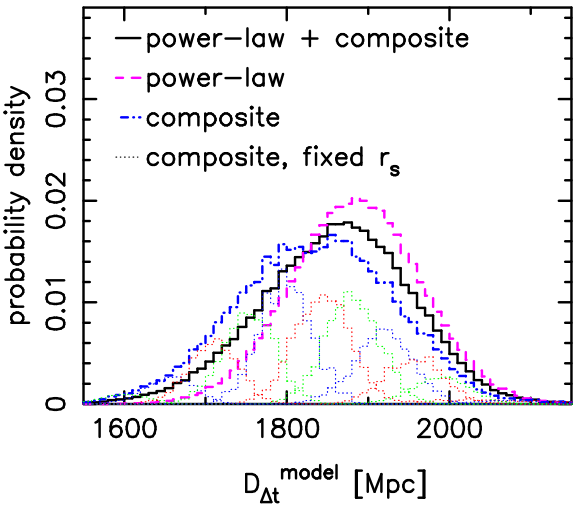

FIG. 3.— The modeled time-delay distance, $D_{\Delta t}^{\rm model}$, for the power-law model (dashed) and the composite model of baryons and dark matter (dot dashed). The dotted color curves correspond to different $r_{\rm s}$ chains, weighted by the time-delay likelihood. The solid curve is the combined $D_{\Delta t}^{\rm model}$ by weighting the two models equally. The PDFs of the combined, power-law and composite models have been scaled by a factor of 4 for clarity.

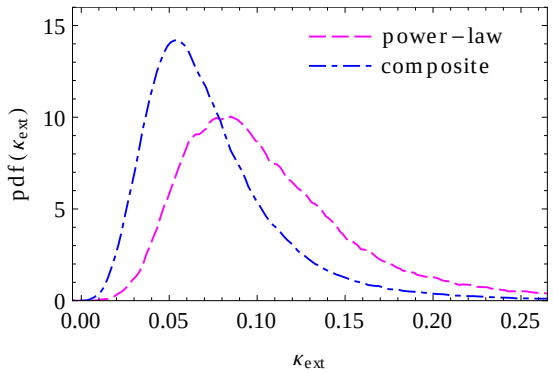

FIG. 4.— The PDF for the external convergence $\kappa_{\rm ext}$ from combining ray tracing through the Millennium Simulation with (1) the galaxy count around the lens system that is 1.4 times the average number of galaxy counts, and (2) the modeled external shear. The composite model with $\gamma_{\rm ext} = 0.070 \pm 0.004$ is in dot-dashed, and the power-law model with $\gamma_{\rm ext} = 0.089 \pm 0.006$ (SU13) is in dashed.

$$\frac{1}{\sqrt{2\pi}(x-\lambda_{\rm D})\sigma_{\rm D}} \exp\left[-\frac{(\log(x-\lambda_{\rm D})-\mu_{\rm D})^2}{2\sigma_{\rm D}^2}\right], \quad (5)$$

where $x = D_{\Delta t}/(1\,{\rm Mpc})$, $\lambda_{\rm D} = 1362.5$, $\mu_{\rm D} = 6.5433$ and $\sigma_{\rm D} = 0.20033$. Our inference of $D_{\Delta t}$ is accurate to $\sim 6.5\%$, including the known uncertainties.

4. COSMOLOGY WITH TIME-DELAY LENSES AND THE CMB

The time-delay distance allows us to infer cosmological parameters. We consider four background cosmological models based on the recent results from WMAP9 (Hinshaw et al. 2012) and Planck (Planck Collaboration et al. 2013): (1) WMAP9 open ΛCDM, (2) WMAP9 wCDM, (3) Planck open ΛCDM, and (4) Planck wCDM. Compared to the flat ΛCDM model, open ΛCDM allows for spatial curvature $\Omega_{\rm k}$, and wCDM allows for a time-independent w that is not fixed to -1. We consider these more generic models given the current tensions in H_0 measurements from Planck in flat ΛCDM cosmology and from direct probes (Planck Collaboration et al. 2013).

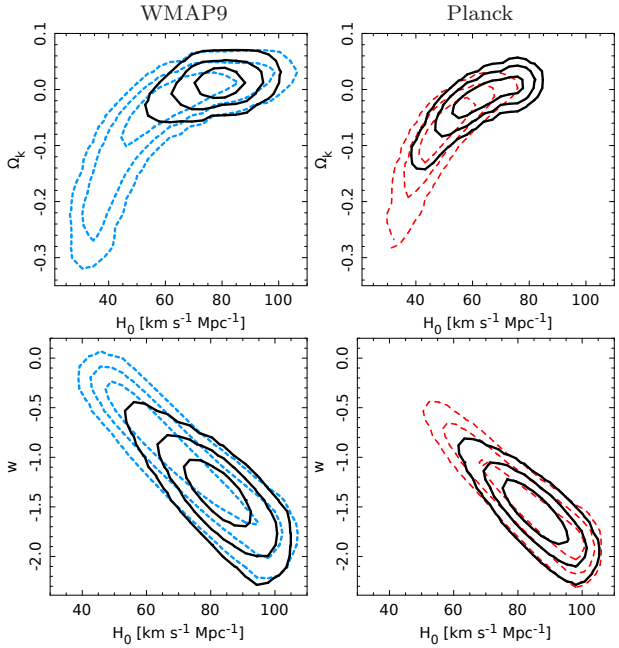

FIG. 5.— Cosmological constraints assuming open ΛCDM (top) and wCDM (bottom). Left/Right panels: WMAP9/Planck priors are shown in dashed, and the combination of RXJ1131−1231 with WMAP9/Planck is in solid. RXJ1131−1231, which primarily constrains H_0, helps break parameter degeneracies in the CMB to determine flatness and w.

For each of the four cosmological priors, we importance sample the WMAP9/Planck MCMC chains (Lewis & Bridle 2002; SU13) with the likelihood of the RXJ1131−1231 data from our improved analysis. In Figure 5, we show the cosmological constraints from the combination of RXJ1131−1231 with WMAP9 (left-hand panels) or with Planck (right-hand panels) in solid contours. Compared to the WMAP9-only or Planck-only constraints (dashed), the gravitational lens RXJ1131−1231 reduces the parameter degeneracies in the CMB data.

The marginalized joint constraints in open ΛCDM are

$$\begin{cases} H_0 = 79.0^{+4.7}_{-5.0}\,{\rm km\,s^{-1}\,Mpc^{-1}} \\ \Omega_{\rm k} = 0.012^{+0.006}_{-0.007} \end{cases} \quad \text{(WMAP9 + RXJ1131)}$$

and

$$\begin{cases} H_0 = 63.9^{+8.9}_{-7.7}\,{\rm km\,s^{-1}\,Mpc^{-1}} \\ \Omega_{\rm k} = -0.01 \pm 0.02 \end{cases} \quad \text{(Planck + RXJ1131).}$$

The marginalized joint constraints in the flat wCDM model are

$$\begin{cases} H_0 = 82.5^{+6.5}_{-6.3}\,{\rm km\,s^{-1}\,Mpc^{-1}} \\ w = -1.36^{+0.20}_{-0.22} \end{cases} \quad \text{(WMAP9 + RXJ1131)}$$

and

$$\begin{cases} H_0 = 85.3^{+6.5}_{-5.9}\,{\rm km\,s^{-1}\,Mpc^{-1}} \\ w = -1.55^{+0.19}_{-0.21} \end{cases} \quad \text{(Planck + RXJ1131).}$$

The difference in the above marginalized H_0 with Planck in the two cosmologies is driven by the Planck data.

5. DISCUSSIONS AND CONCLUSION

The two dominant sources of uncertainty in determining $D_{\Delta t}$ originate from (1) the radial profiles of the lens mass distribution in the region spanned by the images, and (2) weak lensing effects due to mass structures along the line of sight. Recently, SS13 considered toy models of spherical lens mass distributions with point-like sources and suggested that lens models with different radial profiles can lead to $D_{\Delta t}$ values that differ by $\sim 20\%$ while fitting to the point-like images. We have considered their two lens density profiles in an improved analysis of RXJ1131−1231, and have demonstrated that the *spatially extended Einstein ring of the lensed source* and the availability of multiple time delays provide strong constraints on the *local* profile of the lens mass distribution (see Figure 2). By combining estimates of the external convergence $\kappa_{\rm ext}$ from the lens environment with the modeled external shear, we break some of the parameter (mass-sheet) degeneracy in the lens model, and show that the results are robust with respect to the chosen form of mass profile at large radii (close to isothermal versus NFW). Work is underway to improve estimates of $\kappa_{\rm ext}$ (e.g., Greene et al. 2013; Collett et al. 2013).

The various lens model assumptions lead to similar $D_{\Delta t}$, within 3%, given the exquisite data set. We give a fitting formula in Equation (5) for the PDF of the inferred $D_{\Delta t}$ to RXJ1131−1231 that can be combined with any independent probe of cosmology.

In the composite model of baryons and an NFW halo, $D_{\Delta t}$ is correlated with $r_{\rm s}$ of the halo: higher $r_{\rm s}$ leads to higher $D_{\Delta t}$. Only a range of $r_{\rm s}$ values is compatible with the observed time delays. In particular, the time delays constrain $r_{\rm s} = 7\farcs5 \pm 0\farcs9$ (approximately $32 \pm 4\,$kpc).

By modeling the baryons separately from the dark matter halo, we obtain a rest-frame $M/L_{\rm V} = 5 \pm 2\,M_\odot/L_{\rm V,\odot}$ for the baryonic component, where the uncertainty stems mainly from the extrapolation of the lens light profile at large radii. The dark matter mass fraction ($f_{\rm DM}$) within the lens galaxy effective radius of $1\farcs85$ is $\sim 40\%$. These values are typical of massive early-type galaxies (e.g., Auger et al. 2010; Barnabè et al. 2011). As seen in Figure 2, neither the dark matter nor the baryons is a power law, but the combination of the two leads to a nearly perfect power law locally. This "bulge-halo conspiracy" has already been noted in earlier studies (e.g., Treu & Koopmans 2004; Koopmans et al. 2009; van de Ven et al. 2009) and is reproduced by some numerical simulations including baryonic physics (Remus et al. 2013).

The inferred H_0 value from Planck in the flat ΛCDM model is $67.3 \pm 1.2\,{\rm km\,s^{-1}\,Mpc^{-1}}$. This is in tension with several direct H_0 probes, including the Cepheids distance ladder with $H_0 = 73.8 \pm 2.4\,{\rm km\,s^{-1}\,Mpc^{-1}}$ (Riess et al. 2011) or $H_0 = 74.3 \pm 0.4\,({\rm stat.}) \pm 2.1\,({\rm sys.})\,{\rm km\,s^{-1}\,Mpc^{-1}}$ (Freedman et al. 2012). Our measurement of H_0 from RXJ1131−1231 (with WMAP9 priors) is also in tension with the Planck value under the flat ΛCDM assumption. We emphasize that the H_0 measurements from the CMB are highly model-dependent; the value of H_0 can change markedly when one relaxes from spatial flatness or Λ, as illustrated in Figure 5. The currently perceived tension could be due to unknown systematic uncertainties or an indication of new physics such as the dark energy component not having $w = -1$. It is now crucial to pin down the uncertainties of each approach and employ multiple independent probes to rule out unknown systematics.

Gravitational lens time delays provide an independent one-step method to determine cosmological distances. With extensive data sets on RXJ1131−1231, we measure its $D_{\Delta t}$ to a precision of 6.5% including uncertainty between different simply-parameterized lens models. We will soon have three more time-delay lenses with similar data quality as that of RXJ1131−1231 and B1608+656 to reduce our statistical uncertainties on cosmological parameters, and more importantly, to test for the presence of residual systematics in our approach. By understanding the origin of our systematic uncertainties, the statistical power of the hundreds of time-delay lenses that will be discovered in current and upcoming surveys will be realized (e.g., Treu et al. 2013). We are entering an exciting era of *accurate* cosmology as various methods begin to gain both the precision and accuracy required to rule out cosmological models and potentially discover new physics.

ACKNOWLEDGMENTS

We thank Adriano Agnello, Peter Schneider, Dominique Sluse, and Kenneth Wong for useful discussions. We acknowledge support by NASA through *HST* grant GO-12889. T.T. acknowledges support from the Packard Foundation. R.D.B. acknowledges support by the National Science Foundation (NSF) grant number AST-0807458. F.C., G.M., and M.T. acknowledge support from the Swiss National Science Foundation. C.D.F. acknowledges support from NSF-AST-0909119. This paper is based in part on observations made with the NASA/ESA *HST*, obtained at the Space Telescope Science Institute, which is operated by the Association of Universities for Research in Astronomy, Inc., under NASA contract NAS 5-26555. These observations are associated with program GO-9744.

REFERENCES

Auger, M. W., Treu, T., Bolton, A. S., et al. 2010, ApJ, 724, 511
Barnabè, M., Czoske, O., Koopmans, L. V. E., Treu, T., & Bolton, A. S. 2011, MNRAS, 415, 2215
Chávez, R., Terlevich, E., Terlevich, R., et al. 2012, MNRAS, 425, L56
Claeskens, J.-F., Sluse, D., Riaud, P., & Surdej, J. 2006, A&A, 451, 865
Collett, T. E., Marshall, P. J., Auger, M. W., et al. 2013, MNRAS, 432, 679
Courbin, F., Chantry, V., Revaz, Y., et al. 2011, A&A, 536, A53
Dutton, A. A., Brewer, B. J., Marshall, P. J., et al. 2011, MNRAS, 417, 1621
Fassnacht, C. D., Koopmans, L. V. E., & Wong, K. C. 2011, MNRAS, 410, 2167
Freedman, W. L., Madore, B. F., Scowcroft, V., et al. 2012, ApJ, 758, 24
Gavazzi, R., Treu, T., Rhodes, J. D., et al. 2007, ApJ, 667, 176
Golse, G., & Kneib, J.-P. 2002, A&A, 390, 821
Greene, Z. S., Suyu, S. H., Treu, T., et al. 2013, ApJ, 768, 39
Hilbert, S., Hartlap, J., White, S. D. M., & Schneider, P. 2009, A&A, 499, 31
Hinshaw, G., Larson, D., Komatsu, E., et al. 2012, ArXiv e-prints (1212.5226)
Humphrey, P. J., & Buote, D. A. 2010, MNRAS, 403, 2143

Kochanek, C. S., Morgan, N. D., Falco, E. E., et al. 2006, ApJ, 640, 47
Koopmans, L. V. E. 2004, ArXiv e-prints (astro-ph/0412596)
Koopmans, L. V. E., Treu, T., Bolton, A. S., Burles, S., & Moustakas, L. A. 2006, ApJ, 649, 599
Koopmans, L. V. E., Bolton, A., Treu, T., et al. 2009, ApJ, 703, L51
Lewis, A., & Bridle, S. 2002, Phys. Rev. D, 66, 103511
Navarro, J. F., Frenk, C. S., & White, S. D. M. 1996, ApJ, 462, 563
Planck Collaboration, Ade, P. A. R., Aghanim, N., et al. 2013, ArXiv e-prints (1303.5076)
Reid, M. J., Braatz, J. A., Condon, J. J., et al. 2013, ApJ, 767, 154
Remus, R.-S., Burkert, A., Dolag, K., et al. 2013, ApJ, 766, 71
Riess, A. G., Macri, L., Casertano, S., et al. 2011, ApJ, 730, 119
Sand, D. J., Treu, T., Ellis, R. S., Smith, G. P., & Kneib, J.-P. 2008, ApJ, 674, 711
Schneider, P., & Sluse, D. 2013, ArXiv e-prints (1306.0901)
Sluse, D., Surdej, J., Claeskens, J.-F., et al. 2003, A&A, 406, L43
Springel, V., White, S. D. M., Jenkins, A., et al. 2005, Nature, 435, 629
Suyu, S. H., Marshall, P. J., Blandford, R. D., et al. 2009, ApJ, 691, 277
Suyu, S. H., Treu, T., Blandford, R. D., et al. 2012, ArXiv e-prints (1202.4459)
Suyu, S. H., Auger, M. W., Hilbert, S., et al. 2013, ApJ, 766, 70
Tewes, M., Courbin, F., & Meylan, G. 2013, A&A, 553, A120
Tewes, M., Courbin, F., Meylan, G., et al. 2012, ArXiv e-prints (1208.6009)
Treu, T., & Koopmans, L. V. E. 2004, ApJ, 611, 739
Treu, T., Marshall, P. J., Cyr-Racine, F.-Y., et al. 2013, ArXiv e-prints (1306.1272)
van de Ven, G., Mandelbaum, R., & Keeton, C. R. 2009, MNRAS, 398, 607